Global NEST Journal, Vol 25, No X, pp 151-168

Batch and packed bed column studies of azo dyes adsorption from the aqueous solutions using activated sugarcane bagasse charcoal adsorbent: isotherm and kinetic studies

Hariharan T.[1], Gokulan R.[2], Venkat Saravanan R.[3], Zunaithur Rahman D.[4]*
[1]Department of Chemical Engineering, Mohamed Sathak Engineering College, Kilakarai 623806, Tamil Nadu, India
[2]Department of Civil Engineering, GMR Institute of Technology, Srikakulam 532127, Andhra Pradesh, India
[3]Department of Civil Engineering, Velammal College of Engineering and Technology, Madurai 625009, Tamil Nadu, India
[4]Department of Civil Engineering, Aalim Muhammed Salegh College of Engineering, Avadi, Chennai 600055, India
Received: 22/09/2022, Accepted: 20/10/2022, Available online: 31/10/2022
*to whom all correspondence should be addressed: e-mail: zunaithur@gmail.com
https://doi.org/10.30955/gnj.004492

Graphical abstract

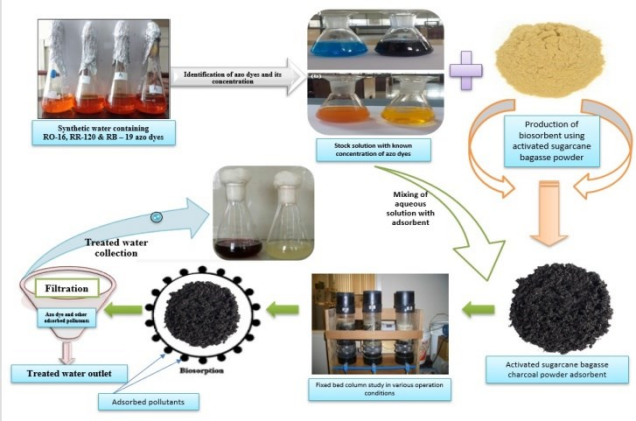

Abstract

Biosorption of azo dyes (RO-16, RB-120 & RB-19) from the aqueous solutions was investigated using the activated sugarcane bagasse charcoal adsorbent. The characteristics of the prepared adsorbent were analyzed by SEM, EDX, FTIR, XRD, TG & DT analysis, and the BET surface area of the sugarcane bagasse adsorbent was examined by N_2 adsorption and desorption techniques. Batch adsorption studies were performed to determine the optimum pH, azo dye concentration, sugarcane dose & temperature, and both Langmuir & Freundlich isotherm studies fit well with the adsorption process. Packed bed column adsorption studies confirmed the earlier breakthrough of the adsorption process, and the column adsorption studies fitted with Thomas, Yoon-Nelson, BDST and Adams-Bohart models. The desorption studies were conducted by adding various concentrations of sulfuric acid, and regeneration of spent azo dyes was done by different cycles.

Keywords: Azo dyes, batch and column studies, sugarcane bagasse, isotherm and kinetic studies, desorption and Regeneration

1. Introduction

Water, Air, and Soil are the most precious natural resources to all substances for living and biological activity on the earth. Among these three, water is one of the essential resources required for every process worldwide. In earlier stages, the water is in an inexhaustible location, and the availability of fresh water is very high due to the presence of various natural and artificial water resources. Recently, freshwater has been required for all significant activities, industrial operations, drinking purposes, etc., and the freshwater requirement is increasing daily because of the need. At the same time, this water gets polluted by various industrial activities, population growth, and other natural or artificial disasters. Environmental pollution has emerged in the past few decades, which may severely affect all living beings (Briffa *et al.*, 2020). There are many industries, and the industrial effluent has toxic pollutants, and without any prior treatment, the effluent was discharged into the natural water sources. Textile industries create too large amounts of effluent with toxic nature (Yaseen *et al.*, 2018). Water treatment is one of the emerging technologies developed recently to remove harmful pollutants from aqueous solutions. Dyes play a vital role in the textile industrial effluent, creating aquatic toxicity and severe health issues. Removing these toxic pollutants is a critical task for researchers, and many industries must bear very high capital and investment costs for the treatment.

Preliminary, Secondary, and biological treatment processes were not suitable for removing the toxic contaminants and other pollutants from the industrial effluent (Shindhal *et al.*, 2020). Due to urgent need, an innovative treatment method is necessary for treating the effluent. Many treatment methods are available, such as Adsorption, Ion exchange, Membrane filtration, Chemical precipitation, etc., to remove or reduce the toxicity level in the industrial effluent (Sathya *et al.*, 2022). The capital and investment costs for adopting these methods are very high, and there

is also a possibility of generating secondary pollutants from the treatment. Among these treatment methods, adsorption is the most straightforward process for reducing the concentrations of contaminants in the industrial effluent (Gisi *et al.*, 2016). It is the process of attracting pollutants from the aqueous medium due to the wan-der-walls interactions. Adsorption offers various advantages, including inexpensive capital and maintenance costs, selective pollutant removal, ease of planning and operation, and the formation of no hazardous chemical contaminants. But it has some disadvantages like the cost of adsorbent, low surface area, skilled labour requirement, etc. Adsorption using activated carbon is one of the emerging technologies in recent days (Sultana *et al.*, 2022). Many organic/inorganic materials were used as an adsorbent for removing the pollutants and other toxic contaminants from an aqueous solution. The adsorbent is the material that is commonly used in the adsorption process to adsorb the impurities from the sources.

Table 1. List of research work conducted for azo dyes removal using sugarcane bagasse

S. No.	Type of azo dye	The efficiency of azo dye removal	Azo dye concentration	Optimum pH	Optimum dose	Optimum bed height	Optimum flow rate	Reference
1.	RO-16, RR-120 & RB-19	95%, 88% & 82%	25 mg L^{-1}	6.0	2.5 g L^{-1}	10 cm	5 mL min^{-1}	This study
2.	MB	97%	25 mg L^{-1}	7.5	0.5 g	-	-	Kerrou *et al.*, 2021
3.	MG	89.60%	8 x 10^{-6} M	7.0	0.3 g	-	-	Tahir *et al.*, 2016
4.	RB & MB	0.19 & 0.35 mmol	3 x 10^{-4} mol L^{-1}	6.5	1.0 g	12.5 cm	4.5 mL min^{-1}	Xia Yu *et al.*, 2019
5.	BB, MB & BY	87.12%, 74.31% & 79.28	5 mg L^{-1}	7.5	1.0 g	24 cm	7 mL min^{-1}	Cheong Khoo *et al.*, 2012
6.	Phenol	76.85%	0.22 $mmol^{-1}$	4.5	1.005 mmol g^{-1}	32 mm	2.5 mL min^{-1}	Fideles *et al.*, 2019
7.	SMX	74%	5 mg L^{-1}	6.0	6.4 g	25 cm	2 mL min^{-1}	Juela *et al.*, 2021

Table 2. Properties of activated sugarcane bagasse charcoal adsorbent

S. No.	Physical properties	Activated sugarcane bagasse charcoal
1.	Specific Gravity	0.62
2.	Buk density - g cc^{-1}	0.42
3.	Porosity - %	92
3.	Surface area - $m^2 g^{-1}$	31
5.	Avg. Particle size - µm	0.7–0.525
6.	Moisture content - %	41.3
7.	Ignition loss - w/w %	94.14
8.	Al_2O_3 - w/w %	1.9
9.	SiO_2 - w/w %	0.95

In this study, the activated sugarcane bagasse charcoal has been used for removing the azo dyes from the textile industrial effluents. After extracting juices, the biomass was produced, called the bagasse, usually available in a fiber state. 100 kg of sugarcane was made of around 35 kilograms of bagasse waste from the industrial process, and these decomposable fibers have been used to produce enzymes and biodiesels (Biz *et al.*, 2016). The period of decomposition of this sugarcane bagasse is around 50–60 days, and these are eco-friendly materials available at a low cost. Disposing of these bagasse fibers is one of the challenging tasks, and handling is also a complicated process. Based on the above statements, it is decided to remove the azo dye concentrations using the activated sugarcane bagasse charcoal as an adsorbent material. For preliminary investigation purposes, the list of research works conducted for the adsorption of various dyes using sugarcane bagasse is listed in Table 1. In this research work, the azo dyes such as reactive orange (RO-16), reactive red (RR-120) & reactive blue (RB-19) and their adsorption using the biochar obtained from sugarcane bagasse were examined using the fixed-bed column study. The desorption and regeneration studies evaluated the fixed bed column's performance.

2. Materials and methods

2.1. Sugarcane bagasse – adsorbent preparation

The adsorbent material of sugarcane bagasse was collected from the sugar mill industries and washed several times with double distilled water to remove the dust and impurities. Then the washed bagasse samples were kept in an oven at 60°C for 24 hours to remove the tannins and organic solvents. The sample was collected from an oven, washed multiple times, and dried in sunlight. The stability of the sugarcane fiber was increased by adding treated

formaldehyde with a 1:4 ratio (Sugarcane bagasse: Formaldehyde, w/v), and the mixed solution was kept in a muffle furnace for heating. After 6 hours of boiling time at 100°C), the water evaporated, and the sample was collected and dried in an oven at 80(C) for 24 hours. The physical properties of activated sugarcane bagasse charcoal powder are represented in Table 2.

2.2. Stock solution preparation

The azo dyes of reactive orange 16, reactive red 120 and reactive blue 19 were procured from the local vendors and stored in a refrigerator under a controlled temperature. The cleaning process is not required because of an analytical grade of azo dyes, commonly used in all textile and fabric industries (Xiao *et al.*, 2017). The azo dyes act as a colouring agent in textile processing industries, creating toxic effects on all living beings. In batch and fixed bed column adsorption studies, all three types of dyes were added in double distilled water separately with a concentration of 1000 ppm.

2.3. Characterization of adsorbent

Material characteristics studies were performed to evaluate the properties of prepared adsorbent from the sugarcane bagasse charcoal by chemical synthesis process. The subsequent characterisation studies were used to determine the adsorption behaviour of the sugarcane bagasse-activated charcoal powder.

2.3.1. BET surface area analysis

The adsorption of a gas on the solid surface of activated sugarcane bagasse charcoal was used to identify the adsorbent's pore volume & size, and surface area. The quantity of adsorbate gas associated with a monomolecular layer on the surface was calculated. Due to the relative van der walls forces between the sugarcane bagasse charcoal powder and gas molecules, physical adsorption was attained (Guo *et al.*, 2020). The surface area determination was carried out at the liquid nitrogen and its temperature. The multilayer adsorption of nitrogen obtained the specific surface area of the prepared sugarcane bagasse charcoal adsorbent as a function of relative pressure (P/P_o). The volume of micro and meso pores of the sugarcane bagasse charcoal adsorbent was obtained using the t-plot method. The BET isotherm can be an expression in the equation (1).

$$\frac{1}{V_a\left(\frac{P_o}{P}-1\right)}=\frac{C-1}{V_mC}X\frac{P}{P_o}+\frac{1}{V_mC} \quad (1)$$

Here, P is adsorbate gas partial vapour pressure in pascals, P_o is adsorbate gas saturated pressure in pascals, V_a is the volume of gas adsorbed in the standard temperature and pressure, and V_m is the volume of gas adsorbed for producing monolayer on the adsorbent surface at standard temperature and pressure. C is the constant for enthalpy of adsorption.

2.3.2. SEM/EDX analysis

Using the SEM-EDX spectroscopy (JSM – 6940V), sugarcane bagasse charcoal's physical and elemental properties have been evaluated. By SEM analysis, the fractions and flaws, contaminants and other organic and inorganic particles were observed with a working distance of 10 µm and a voltage level of 20 kV. The adsorbent material was taken in two SEM images before and after receiving the pollutants. The adsorption of targeted azo dyes was identified by referring to the EDX instrumental analyses performed with SEM.

2.3.3. XRD

X-ray Diffraction analysis was used to analyze the crystalline structure of the adsorbent material at the different peaks. The phases and sizes of the crystalline structure were identified by operating the instrument with CuK – α – radiation and the power of 40 kV working at 250 mA. The characteristics of peaks were obtained from the analysis and compared with JCPDS standards using the reference code of -00-002-1035 (Harripersadth *et al.*, 2020).

2.3.4. FTIR analysis

The different types of functional groups (Hydroxyl, Carbonyl, etc.) and their presence in the prepared sugarcane bagasse adsorbent were examined by FTIR studies. In this experimental work, 1 gm of activated charcoal sugarcane bagasse powder was taken and mixed with 100 mg L^{-1} of azo dye concentrated synthetic solution with a pH of 6.0. After 4 hours of agitation, the supernatant was collected and used for further experimental study. The resolution was fixed at 4 cm^{-1} with a scanning range from 4000 cm^{-1} to 400 cm^{-1}. Twenty scans were taken to obtain the spectra. The spectra were obtained before and after the adsorption of pollutants from the synthetic solutions.

2.3.5. TGA & DTA

Thermo-Gravimetric and Derivative Thermogravimetric studies were utilized to determine the adsorbent's mass and energy changes at high temperatures. The TGA analysis will determine the quantity of material eliminated from the adsorbent as the temperature rises (Bazan *et al.*, 2016). The DTG study will examine the extraction efficiency of materials within the expected time to determine if the adsorption process is exothermic or endothermic. To get the TGA and DTG characteristics, 20 mg of adsorbent material was placed in the instrument for characterization.

2.4. Batch adsorption studies

The batch adsorption method was used to evaluate the adsorption of azo dyes using activated sugarcane bagasse powder by altering pH levels, adsorbent dose, concentrations, period of contact with adsorbent, and solution temperature. The following adsorption process parameters were changed in this experimental work: The pH of the synthetic solution (2.0 to 7.0), contact time (10 to 120 min), adsorbent dosage (0.5 to 2.5 g L^{-1}), azo dye concentration (25 to 150 mg L^{-1}), and temperature (15 to 60°C). The produced adsorbent was put into known concentrations of synthetic solutions. The conical flask was continuously shaken in the rotary shaker for 60 minutes to

achieve equilibrium. Equation 2 was used to compute the amount of azo dye adsorbed by the adsorbent.

$$q_t = \frac{(C_o - C_t)\,V}{m}\ mg/g \qquad (2)$$

In this equation, q_t is the quantity of azo dyes adsorbed by sugarcane bagasse at a time 't,' and C_t denotes the batch adsorption study concentration. After 5 minutes of centrifugal, the final suspension was removed from the rotary shaker. Using atomic adsorption spectroscopy, the quantity of azo dyes adsorbed after the adsorption process was determined. Each analysis was conducted twice to obtain the current value, and the average value was used. The quantity of azo dyes eliminated by sugarcane bagasse may be determined using data from the batch studies. Equation 3 may be used to define the mass balance system for this adsorption process.

$$\%\ \text{Removal} = \left[\frac{C_o - C_e}{C_o}\right] X100 \qquad (3)$$

Here, C_o denotes the beginning concentration of azo dyes in solution (mg L^{-1}), C_e is the equilibrium concentration of azo dye compounds (mg L^{-1}), V denotes the total volume of solution, and 'm' denotes the mass of the employed adsorbent.

2.5. Batch isotherm studies

The transfer of selected azo dye compounds from the liquid phase to the adsorbent during the static equilibrium has been examined using adsorption isotherm investigations. This may aid in identifying adsorbent interactions and optimizing them during adsorption. The types of isotherm studies listed below are commonly used to evaluate the efficiency of the adsorption mechanism in batch mode.

2.5.1. Langmuir isotherm

The Langmuir isotherm study explained the stability between the adsorbate and adsorbent systems. The isotherm research is based on two principles. The whole adsorption process, in other words, comprises a monolayer on the surface of the adsorbent, and molecular bonding at distinct places is impossible (Al-Senani *et al.*, 2018). Equation 4 expresses the Langmuir isotherm model.

$$\frac{C_e}{q_e} = \frac{1}{K.q_{max}} + \frac{C_e}{q_{max}} \qquad (4)$$

C_e – Solution's concentration during the equilibrium in mg L^{-1}; q_e – Amount of azo dyes adsorbed per gm; K & q_{max} – Constants of Langmuir isotherm equation related to capacity and intensity of adsorption.

2.5.2. Freundlich isotherm

The Freundlich isotherm study can clearly describe the adsorption behaviour of the adsorbent. Freundlich model arises mostly on heterogeneous surfaces and follows the multilayer adsorption system on the surface of the adsorbent (Saadi *et al.*, 2015). Equation 5 expresses the Freundlich isotherm model.

$$\ln q_e = \ln k_f + \frac{1}{n}\ln C_e \qquad (5)$$

q_e – Adsorbed quantity of adsorbate per gm; n – Adsorption Energy; K_f – Capacity of adsorption related to Freundlich constant; C_e – Adsorbate solution's equilibrium concentration.

2.5.3. Sips isotherm

The Freundlich and Langmuir models were integrated to forecast the adsorption mechanism in the homogeneous mixed isotherm system. When the solution concentration is relatively high, the sips model predicts monolayer adsorption (Tzabar *et al.*, 2016). Furthermore, the solution's concentration is fully avoided and adheres to the Langmuir isotherm model. Equation 6 presents the expression for the sips isotherm model.

$$\frac{1}{q_e} = \frac{1}{Q_{max}K_s}\left(\frac{1}{C_e}\right)^{\frac{1}{n}} + \frac{1}{Q_{max}} \qquad (6)$$

Q_{max} & K_s – Adsorption capacity and equilibrium constant obtained from the slope and intercept in linear plots & n - factor of heterogeneity lies between 0 to 1.

2.6. Fixed bed column studies

Figure 1 shows a glass column with an internal diameter of 2 cm and an overall length of 30 cm used for fixed bed experimentation and analysis. The characteristics of the fixed bed column (depth of bed, flow rate, and azo dye concentrations) were modified under normal circumstances to assess the column's performance. For the complete analysis, the adsorbent bed depth was varied to 5, 7.5, and 10 cm, and the flow rate of the azo dyes solution was adjusted from 5 to10 mL min^{-1}. The concentration of azo dyes ions was adjusted to 100, 200, and 300 mg L^{-1}. Thomas, Yoon–Nelson, BDST, Adams-Bohart and Wolborska model investigations were carried out for equilibrium studies. To conduct the desorption investigations, concentrated sulfuric acid with different normality (0.1, 0.2, and 0.3) was employed, and the adsorbed dyes were disposed of by remote landfilling.

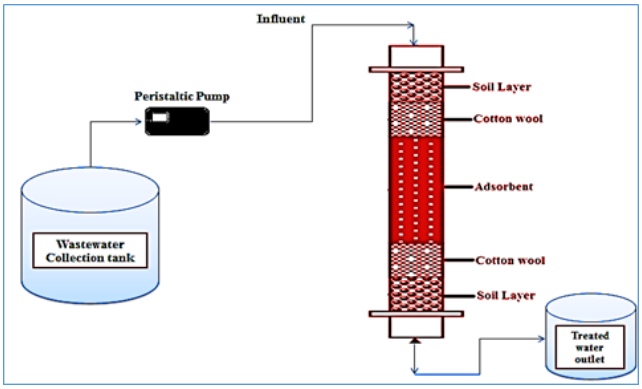

Figure 1. Experimental setup of fixed bed column

To perform the breakthrough analysis of the fixed bed column, the following equations (7 to 11) were used.

$$q_{total} = \frac{Q}{1000}\int_{t=0}^{t_{total}} C_{ad}\,dt \quad (7)$$

$$V_t = Qt_{total} \quad (8)$$

$$q_{bed} = \frac{q_{total}}{W} \quad (9)$$

$$M_{total} = \frac{C_0 Q t_{total}}{1000} \quad (10)$$

$$\%removal = \frac{q_{total}}{M_{total}} * 100 \quad (11)$$

Here, $q_{total-the}$ amount of azo dyes uptake by the sugarcane bagasse adsorbent in the packed bed column in mg; C_o – Concentration of azo dyes during the initial time in mg L^{-1}; C_{ad} – The difference between initial and final azo dye concentration at the flow time in mg L^{-1}; V_t – Volume of synthetic solution after the treatment; Q – The rate of volumetric flow (mL min^{-1}); T_{total} – Flow time in total; q_{bed} – adsorbent bed capacity in mg g^{-1}; W – Weight of the sugarcane bagasse charcoal in gm; M_{total} – Amount of azo dyes in the column.

2.7. Kinetic modelling

It is very important to predict the breakthrough curve for the parameters of effluents in the fixed bed column process. The column's dynamic behaviour was predicted using the following five types of kinetic models.

2.7.1. Thomas model

Thomas model has been widely used to examine column performance and to investigate the forecast of fixed bed column breakthrough curves (Amiri *et al.*, 2019). The main assumption of this model is that plug flow dispersion predominates in the adsorption bed. This model can be expressed in equation (12).

$$\ln\left(\frac{C_o}{C_i} - 1\right) = \frac{K_{th} q_o w}{Q} - K_{th} C_o t \quad (12)$$

The Thomas model parameters of K_{th} & q_o were calculated from the slope and intercepted values of the plot ln ((C_o/C_i) – 1)) vs time. C_i is called the concentration of the solution in mg L^{-1}, K_{th} is the constant of the Thomas model in L mg^{-1} min^{-1}, q_o is the concentration of the solute at the solid phase in mg g^{-1}, w is the mass of adsorbent, Q is the flow rate in mL $min^{-1,}$ and t is the follow time in minutes.

2.7.2. Yoon-Nelson model

The Yoon-Nelson model is simple and relates to a single system component. It does not have quite so many column parameters (Liu *et al.*, 2016). According to the model, the decrease in adsorption probability for increasing adsorbate molecules is substantially related to the possibility of adsorbate breakthrough and adsorbate adsorption. The Yoon - Nelson Model may be stated mathematically as equation (13).

$$\ln\left(\frac{C_i}{C_o - C_i}\right) = K_{YN} t - K_{YN}\tau \quad (13)$$

The slope of straight line K_{YN} and intercept – τ K_{YN} was calculated by plotting $\ln\left(\frac{C_i}{C_o - C_i}\right)$ Vs time. C_i is the solution concentration in mg L-1, Co is the azo dye concentration in mg L^{-1}, K_{YN} is the constant of the Yoon-Nelson model in min^{-1}, τ is the required time of 50% breakthrough in minutes, and t is the flow time in minutes.

2.7.3. BDST model

Based on the forecast of various breakthrough sites, the model determined the adsorption bed capacity. This model's main assumption is that the adsorption rate is regulated by the unused capacity of the adsorbent and the surface response on the adsorbate's surface (Sharifian *et al.*, 2020). The BDST model parameters (N_o and K) were determined by plotting bed depth vs time. The BDST model can be expressed in equation 14.

$$t = \frac{N_0 Z}{C_o V} - \frac{1}{KC_0}\ln\left(\frac{C_o}{C_b} - 1\right) \quad (14)$$

Here, t is called column service time in minutes, N_0 is called the capacity of adsorption bed mg L^{-1}, Z is called the column bed depth in cm, C_0 is called concentration of influent solute in mg L^{-1}, V is called linear flow velocity cm min^{-1}, K is called the rate constant in L mg^{-1} $min^{-1,}$ and C_b is called azo dye breakthrough concentration in mg L^{-1}.

2.7.4. Adams-Bohart model

The main assumption of this kinetic model is that the adsorbent concentration and residual capacity are directly related to the adsorption rate (Saad *et al.*, 2015). At the time of the initial part of the breakthrough curve attainment, this model was used, and the model can be expressed in equation 15.

$$ln\left(\frac{C_t}{C_o}\right) = K_{AB} C_o t - \frac{K_{AB} N_o Z}{F} \quad (15)$$

K_{AB} is the kinetic constant in L mg^{-1} min^{-1}, F is the flow rate in mL min^{-1}, Z is the depth of column bed in cm, N_o – adsorbent's maximum adsorption capacity in mg L^{-1} and t is the time in minutes.

2.7.5. Wolborska model

The distribution of concentrations and dynamics of the adsorption during the initial stages was described by this model in lower concentrations (Djelloul *et al.*, 2014). The constants of the Wolborska model were obtained using the linear plots of ln (C_t/C_o) vs time. The basic assumption of this kinetic model is that the breakthrough curve in the final stage and the concentration profile width are constant. The linear expression of the Wolborska model can be expressed in equation 16.

$$\ln\frac{C}{C_o} = \frac{\beta_a C_o}{N_o} t - \frac{\beta_a Z}{U_o} \quad (16)$$

C is the concentration of effluent in mg L^{-1}, C_o is the concentration of influent in mg L^{-1}, β_a is the mass transfer kinetic coefficient, N_o is the capacity of exchange in mg L^{-1}, U_o is the velocity of the superficial fluid in mm $hr^{-1,}$ and Z is the depth of bed in mm.

2.8. Desorption and regeneration

Reusing spent adsorbent is one of the ecofriendly methods and creates very low toxic effects on the surrounding environment. Concentrated sulfuric acid was employed as a regenerating reagent in this work at various concentrations such as 0.1 M, 0.2 M, and 0.3 M. The desorbing solution was let into the bed in continuous flow at a flow rate of 5 mL min^{-1}, and the solution was collected at the exit point of the fixed bed column every 5 minutes. Finally, the concentration of the solution has been analyzed.

3. Results and discussion

3.1. Pore size and volume distribution

For this porous material, the adsorption-desorption isotherm procedure was utilized to acquire the size of the pore and its volume fraction, BET surface area, and other micro and meso pore of sugarcane bagasse using nitrogen at -196°C. Figure 2 shows the adsorption rate and desorption with nitrogen, and Table 3 represents the experimental parameters. The sugarcane bagasse was discovered to have micro and meso pores (Type - II) and a BET surface area of about 654 m^2/g, which is greater than the pore volume (0.412 cm^3/g) of other conventional carbon materials (Li *et al.*, 2015).

3.2. SEM & EDX analysis

Figure 3 shows the activated sugarcane bagasse charcoal powder's surface before and after the azo dye uptake. Referring to Figure 3 (a), it was seen that a flat nature on the adsorbent's surface with uneven holes before the adsorption of azo dyes. Due to acid treatment of the adsorbent, uneven holes were observed on the surface of the adsorbent (Ambaye *et al.*, 2021). At the same time, Figure 3 (b) shows the cloud nature on the adsorbent surface; most of the holes were filled with pollutants after the adsorption process. This may confirm the process of adsorption was achieved by the prepared sugarcane bagasse charcoal adsorbent.

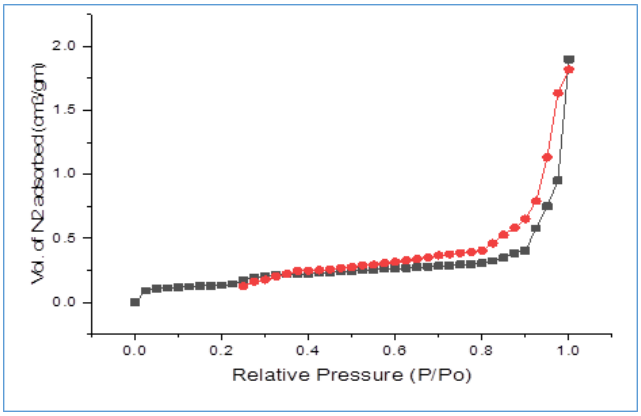

Figure 2. Adsorption – Desorption Isotherm (Nitrogen)

Table 3. Pore characteristics of sugarcane bagasse adsorbent

S. No.	Parameter	Units	Value
1.	BET surface area	$m^2 g^{-1}$	654
2.	Pore volume	$cm^3 g^{-1}$	0.412
3.	Micropore volume	$cm^3 g^{-1}$	0.189
4.	Meso pore volume	$cm^3 g^{-1}$	0.082
5.	Micropore area	$m^2 g^{-1}$	392
6.	Average pore diameter	Nm	0.6–2.4

To confirm the adsorption of targeted azo dyes on the adsorbent surface, EDX analyses were performed. Figure 3 (c) shows the EDX image of the prepared adsorbent before the uptake of azo dyes from the synthetic solution. There are no peaks in the EDX image before adsorbing the targeted azo dyes. But, referring to Figure 3 (d), the presence of various functional groups confirms the adsorption of targeted azo dyes. Along with the dyes, the other organic and inorganic components, such as silica, iron, magnesium, calcium, and other metal elements and components, were observed in the EDX images. At the time of the activated process, the sulfur compound reacted with the adsorbent material and formed many non-ionic functional & hydroxyl groups with cations (Saleem *et al.*, 2019). This is because of the protonation of charged sites at the time of acid treatment, and the sulfuric acid's functional groups were not destroyed.

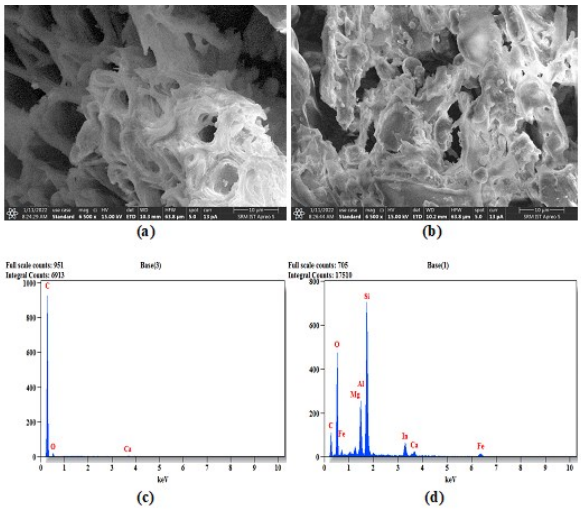

Figure 3. (a) & (b) SEM image of sugarcane bagasse charcoal adsorbent and after the adsorption of azo dyes and (c) & (d) EDX image of sugarcane bagasse charcoal adsorbent and after the adsorption of azo dyes

3.3. XRD analysis

The XRD pattern of activated sugarcane bagasse charcoal adsorbent is shown in Figure 4. From that figure, it was observed many peaks were attained may confirm the crystalline structure of the adsorbent material. The peaks at 160, 240, 280, 311, 395 and 480 at 2θ matches with 80, 110, 60, 40, 35 and 20 hkl planes were good in an agreement that may confirm the crystalline nature. The maximum number of peaks was observed because of the sulfuric acid treatment with the adsorbent material, and the acid may sharpen the peaks with very high intensity.

This suggests that the presence of micro and meso pores in the adsorbent may receive the pollutants from the aqueous medium by physical adsorption and partially by chemical adsorption processes (Nippes *et al.*, 2022). The crystalline structure and peaks at very high intensity may confirm the nature of the prepared adsorbent material.

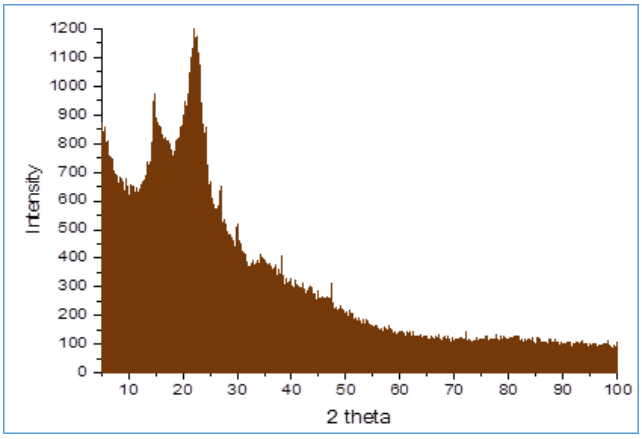

Figure 4. XRD analysis of the activated sugarcane charcoal adsorbent

3.4. FTIR

The functional groups in the sugarcane bagasse charcoal adsorbent were examined by two different types of FTIR images, before and after the azo dye uptake and shown in Figure 5. The -OH and CH_2 groups and their presence was observed by referring to the figure at high energy band of 3420 cm^{-1} and 2860 cm^{-1}. Also, various functional groups were identified between 1800 – 1000 cm^{-1}. i.e., the presence of water was identified at the band level of 1620 cm^{-1}, aromatic vibrations were observed between 1600 – 1460 cm^{-1}, -CH_2 bending vibrations were observed between 1400 – 1380 cm^{-1} and the C-O functional groups were observed due to vibrations at the band level of 1080 cm^{-1}. When the band level reduces from 1000 cm^{-1}, the presence of C-H functional groups was identified because of the aromatic vibrations (Kepenek *et al.*, 2020). The -CH_2 vibration stretching disappeared at 2860 $cm^{-1,}$ and -OH stretching was formed at lower frequency levels (Dittmann *et al.*, 2022). Hence, the FTIR studies confirm the availability of functional groups in the adsorbent and their role in azo dye uptake during the experimental studies.

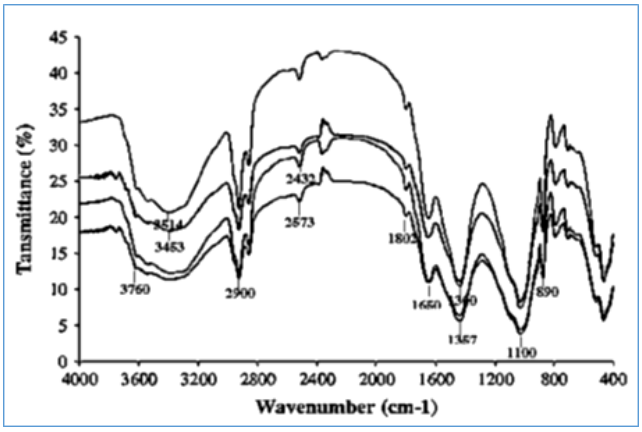

Figure 5. FTIR studies of adsorbent material before and after the adsorption of azo dyes

3.5. TGA & DTA

Figure 6 shows the TG & DT analysis nature of the prepared sugarcane bagasse charcoal adsorbent under various temperatures. It was seen that many functional groups in the adsorbent material. The activated sugarcane bagasse charcoal was exposed to the experimental analysis by adjusting the heat rate of 10°C min^{-1} up to 900°C. Three different stages of adsorbent decomposition represented the heat absorbance of material. The weight loss of the adsorbent material was observed up to the temperature of 600 °C, and after that level, there was no weight loss and attained a constant rate. The sugarcane bagasse adsorbent confirms the endothermic nature because the maximum peak is at 400°C, and the process reaches saturation level at the temperature of 900°C (Venkatraman *et al.*, 2021). The organic and inorganic functional groups and their presence in the adsorbent provide very high stability against the higher temperature.

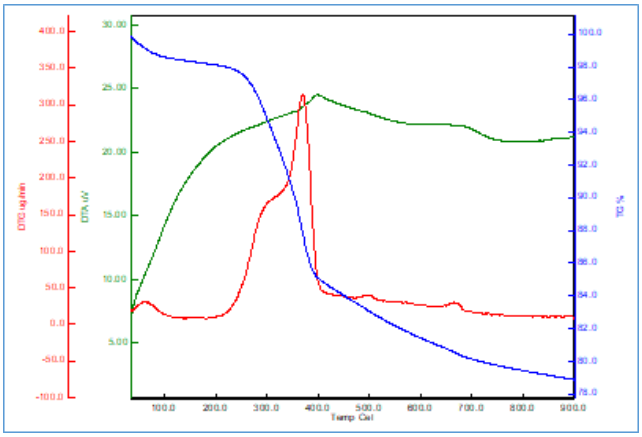

Figure 6. TG & DT analysis of the adsorbent

3.6. Batch adsorption studies

The batch adsorption studies were conducted by adjusting the parameters such as pH, Adsorbent dose, Azo dye concentration, contact time and temperature. The experimental investigations were conducted by varying one parameter and keeping other parameters constant in the aqueous solutions.

3.6.1. pH and its effect

Keeping the adsorption parameters such as azo dye concentration (25 mg L^{-1}), Contact time (60 min) and Sugarcane bagasse dose level (2 g L^{-1}), the impact of the amount of adsorption was examined by adjusting the pH of the solution from 2.0 to 7.0. Figure 7 (a) shows the effect of pH in the azo dye adsorption using the sugarcane bagasse adsorbent. When the pH of the azo dye solution was increased, azo dye uptake also increased. The pH reached a level of 6.0, the maximum adsorption of azo day was achieved and there is a slight decrease when the pH reached 7.0. The pH of azo dye solution goes above 7.0, the surface of the adsorbent has a very high positive charge, and the interaction between azo dyes and the adsorbent has been reduced. The pH of azo dye solution is low, and the positively charged ions on the adsorbent surface protonate for faster removal of azo dyes (Zafar *et al.*, 2019). Due to the hydroxyl precipitation in higher pH values

reduces the azo dye uptake from the synthetic solutions, and the process of adsorption reaches the saturation point at the pH of 6.0 (Gisi *et al.*, 2016). At the optimum pH level, the prepared activated sugarcane bagasse adsorbent removed 95% RO – 16, 88% RR-120 and 82% RB-19 dye concentrations from the synthetic solutions.

3.6.2. Sugarcane dose and its effect

The accessible places on the adsorbent surface decide the degree of adsorption of azo dyes. Also, the adsorbent dosage specifies the available active sites and their significance in the adsorption process during the initial azo dye concentration (Nihan Kaya, 2017). In Figure 7 (b), the maximum azo dye adsorption was achieved by adding 2.5 g L^{-1} of sugarcane bagasse charcoal adsorbent. During the initial stages, the adsorbent dose was added from 0.5 g L^{-1} to 3.0 g $L^{-1,}$ and the effect of adsorption efficiency was investigated. An increase in the amount of azo dye uptake was noticed with an increase in adsorbent dose, and the maximum adsorption was recorded by adding 2.5 g L^{-1} of sugarcane bagasse adsorbent. Around 95% of RO – 16, 84% of RR-120 & 79% of RB – 19 azo dyes were removed from the synthetic solution due to the availability of active sites in the adsorbent.

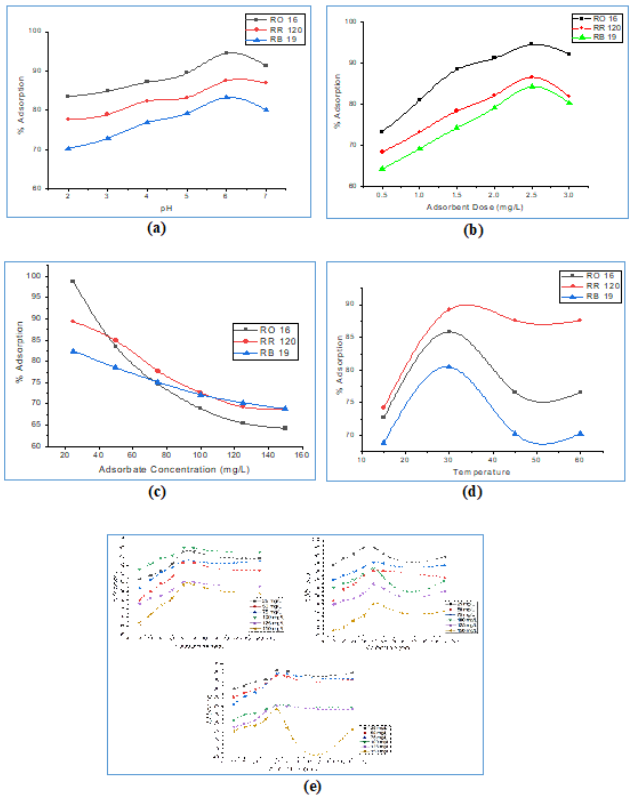

Figure 7. Impact of azo dye adsorption by varying (a) pH, (b) adsorbent dose, (c) Adsorbate concentration, (d) Temperature and (e) Contact time

3.6.3. Azo dye concentrations and their effect

Figure 7 (c) shows the impact of azo dye concentration on the azo dye adsorption in various concentrations. The azo dye concentration was adjusted from 25 mg L^{-1} to 150 mg $L^{-1,}$ and the changes in the amount of azo dye uptake were recorded and represented in that figure. When the concentration of azo dyes in the synthetic solutions was increased, the efficiency of azo dye uptake was reduced gradually because of the degradation of active sites in the sugarcane bagasse adsorbent. Lower concentrations of azo dye solutions with higher sugarcane bagasse dose increase the adsorption efficiency due to the lower number of azo dyes in the synthetic solution (Banerjee *et al.*, 2017). The accessible locations in the sugarcane bagasse adsorbent are directly proportional to the varying azo dye's initial concentration in the aqueous medium. With an increase in azo dye concentration, there is also a decrease in azo dye removal.

3.6.4. Temperature and its effect

Referring to the above batch adsorption studies, the azo dye concentration of 25 mg L^{-1} with 2.5 g L^{-1} of sugarcane bagasse charcoal adsorbent was taken for this experimental study with an optimum pH of 6.0. The temperature of the azo dye solution was adjusted from 15°C to 60°C, and the impact on the azo dye adsorption was examined. Figure 7 (d) shows the effect of adsorption with varying temperatures. When the solution's temperature was increased, there was an increase in azo dye adsorption by the adsorbent noticed (Khamparia *et al.*, 2016). The contact time of this experimental process was fixed at 60 minutes, and the maximum adsorption efficiency was obtained at the temperature of 30°C. A sudden drop in azo dye adsorption was identified when the temperature went above 30°C) because of the desorption rate rise in the solution.

3.6.5. Contact time and its effect

By adjusting the concentrations of azo dyes in the synthetic solutions from 25 mg L^{-1} to 150 mg L^{-1}, the effect of contact time between the adsorbate and adsorbent was investigated. In this study, the contact time was adjusted from 10 minutes to 120 minutes, and the changes in azo dye adsorption efficiency were observed and represented in Figure 7 (e). It was seen that a rapid azo dye uptake happened during the initial stages, and the amount of dye uptake was gradually reduced after 50 minutes of contact time. No significant changes were observed after 50 minutes and the azo dye uptake by the adsorbent reached saturation level. During the initial adsorption process, the availability of vacant sites was high, and the azo dyes were occupied in the vacant sites. During the early period, many unoccupied surface regions are available for adsorption (Ramasamy *et al.*, 2022). Because of the repulsive interactions in the mass process between the solid surface and adsorptive molecules, the resultant unoccupied surfaces are difficult to fill over the period (Staszewski *et al.*, 2022). Azo dye compounds are deposited into mesopores, which become almost full during the initial adsorption phase. As a result, the driving force for the mass transition between the solid phase and the bulk liquid phase decreases and the azo dye particles need to travel deeper with very high resistance.

3.7. Batch isotherm studies

The optimum values were taken from the batch studies, and the isotherm modelling was performed at 30°C by three different methods. The fitting of the isotherm model

was identified based on the slope and intercept & regression values obtained from the linear plots of each model.

3.7.1. Langmuir isotherm

The linear adsorption isotherm plots of Langmuir isotherm studies were shown in Figure 8 (a) by plotting C_e/q_e vs C_e. The constants of this isotherm model 'k and q_{max}' are calculated from the slope and deflection values using the linear plots and listed in Table 4 along with the regression values (R^2). At 30°C, the obtained R^2 values are very high compared to the normal values (< 0.95), which may confirm the applicability of the Langmuir isotherm model. In lower azo dye concentrations (25 mg L^{-1}), the separation parameter values from this study varied from 0 to 1 confirming the adsorption process follows the monolayer formation in either physical or chemical mode (Dey *et al.*, 2022).

Table 4. Isotherm constants for azo dye adsorption using sugarcane bagasse adsorbent

S. No.	Model	Parameters	RO - 16	RR - 120	RB - 19
1.	Langmuir	q_{max}	9.402	9.929	10.434
		K_L	0.343	0.174	0.109
		R^2	0.9721	0.9505	0.9473
2.	Freundlich	K_f	2.541	1.832	1.389
		n	2.963	2.315	2.026
		R^2	0.9546	0.9602	0.9912
3.	Sips	K_S	12.8689	6.13959	3.7113
		β_S	1.25346	1.54742	1.6536
		a_S	0.47347	0.24345	0.1544
		R^2	0.9182	0.9599	0.9991

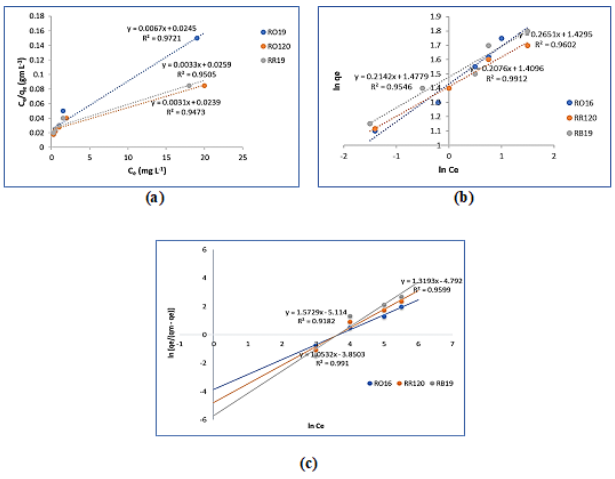

Figure 8. Isotherm study of azo dye adsorption by (a) Langmuir, (b) Freundlich and (c) Sips models

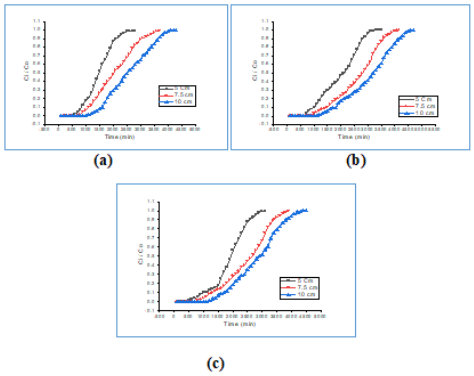

Figure 9. (a), (b) & (c) - Break through curve at different bed depths for RO-16, RR-120 & RB-19 azo dyes adsorption

3.7.2. Freundlich isotherm

For the multilayer adsorption process following through physical or chemical mode, the Freundlich isotherm model was used. Figure 8 (b) shows the linear plots of the Freundlich isotherm model by plotting ln q_e vs ln C_e. The constants of this isotherm model 'K_f and n' are calculated from the slope and deflection values using the linear plots and listed in Table 4 along with the regression values (R^2). At 30°C, the obtained R^2 values are very high compared to the normal values (<0.95) may confirm the applicability of the Freundlich isotherm model. Also, the calculated 'n' values are varied from 1 to 10 may confirm the azo dye adsorption by sugarcane bagasse adsorbent follows physical mode (Krishna Murthy *et al.*, 2020). Regression values (R^2) obtained from the linear plots are above 0.95, confirming the Freundlich isotherm model's best fit. The above isotherm investigations confirm the applicability of both Langmuir and Freundlich models, and the adsorption process follows monolayer and multilayer adsorption by physical or chemical adsorption.

3.7.3. Sips isotherm

*T*he isotherm study derived from both Langmuir and Freundlich models may be used to identify the study's heterogeneous factor. Figure 8 (c) shows the linear plots of the Sips isotherm study by plotting ln [q_e/ (q_m - q_e)] vs ln C_e. The isotherm constants of this model 'Q_{max} and K_s' are calculated from the slope and deflection values from the linear plots and represented in Table 4 along with regression values (R^2). At 30°C, higher regression values were obtained, similar to the Langmuir and Freundlich model, which may confirm this study's applicability. The sips model may reduce to Langmuir or Freundlich isotherm study based on the n values. If the value of n is equal to 1, the model reduces to the Langmuir equation, and if the value of n is equal to 0 the model reduces to the Freundlich equation (Saruchia *et al.*, 2019).

3.8. Breakthrough analysis

The adsorption capacity of sugarcane bagasse adsorbent was determined under the flow conditions; the breakthrough analysis technique was used. In this experimental study, the analysis was evaluated by varying the height of the adsorbent bed, the initial azo dye concentration, and the inflow rate of the solution in the column. The pH and temperature of the solution were kept as a constant value taken from the batch adsorption studies.

3.8.1. Impact of bed height

The azo dye concentration was taken as 50 mg $L^{-1,}$ and the inflow rate of synthetic solution into the column was fixed at 5 mL min^{-1}; the impact was due to the changes in adsorbent bed height in the packed bed column was investigated. In this experimental study, the height of the sugarcane bagasse charcoal adsorbent bed varied from 5 cm, 7.5 cm and 10 cm, respectively, on a trial-and-error basis. Inlet and outlet concentrations of the azo dye solutions were analyzed the sharp curve was developed based on the amount of adsorption and exhaustion time of the adsorbent. Figure 9 (a), (b) and (c) shows the S-shaped breakthrough curve of RO – 16, RR – 120 & RB – 19 azo dyes, respectively. The saturation level of the adsorbent bed was identified at 10 cm bed height, and beyond that, the curve attains the constant removal of azo dyes. The staying time on the adsorbent surface increases in the column and may increase the adsorption rate. Also, the availability of active sites may be occupied by the pollutants, and there is no vacant surface to adsorb the different pollutants (Adeyemo *et al.*, 2015). Because of this reason, the curve attained a constant rate of removal. Hence, it is decided to fix the optimum bed height of 10 cm for further experimental studies. Table 5 represents the calculated parameters by changing the bed height in the packed bed column.

3.8.2. Impact of the flow rate

The adsorbent bed height was fixed at 10 cm, and the concentration of azo dyes in the synthetic solution was kept at 50 mg $L^{-1.}$ The inflow rate of synthetic solution into the packed column was adjusted at various levels. To perform this analysis, the inflow rate was maintained at 5 mL min^{-1}, 7.5 mL min^{-1}& 10 mL min^{-1} on a trial-and-error basis. The flow rate of synthetic solution is directly proportional to the azo dye adsorption. Referring to Figures 9 (a), (b) & (c) – the curve was developed gradually when the flow rate increased and attained the constant rate of azo dye uptake from the aqueous solutions at 10 mL min^{-1}. The breakthrough time was attained at the flow rate of 5 mL min^{-1} during the earlier stages and reached the constant rate. During high flow rate, the turbulence flow in the aqueous solutions plays a vital role, decreasing the rate of azo dye uptake and mass transfer (Benabela *et al.*, 2022). The above investigation confirms the optimum rate of flow in the column is 5 mL min^{-1} for higher efficiency of azo dye uptake. Table 6 represents the values obtained from breakthrough analysis by varying the inflow rate of the azo dye solutions.

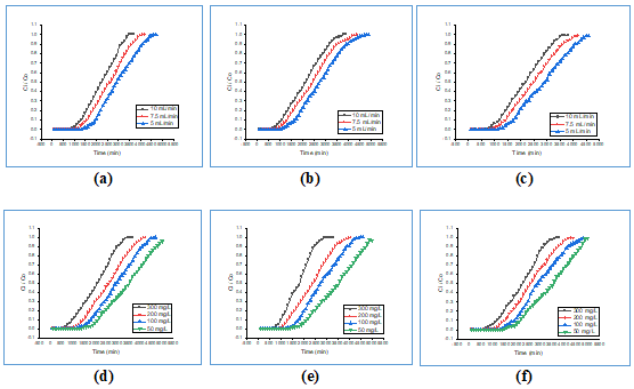

Figure 10. (a), (b) & (c) – Breakthrough curves at different flow rates & (d), (e) & (f) -Breakthrough curves at different concentrations - for RO-16, RR-120 & RB-19 azo dyes adsorption

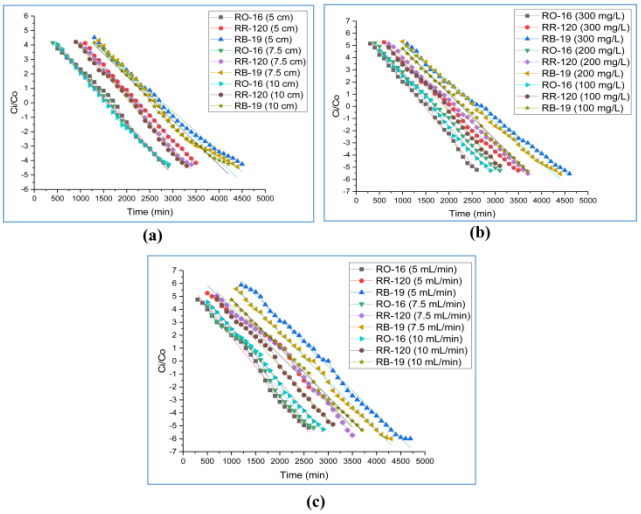

Figure 11. Thomas model plots for (a) different bed depth, (b) azo dye concentration and (c) inflow rate of the synthetic solution in the packed bed column

3.8.3. Impact of azo dye concentrations

The flow rate of azo dye solution was taken as 5 mL $min^{-1,}$ and sugarcane bagasse adsorbent bed height was fixed at 10 cm for this experimental study. The concentration of azo dyes in the synthetic solution varied from 50 mg L^{-1} to 300 mg L^{-1} on a trial-and-error basis. During the initial stages, the breakthrough time was not attained because of the large number of azo dye pollutants and their accumulation. Figure 10 (d), (e) & (f) shows the breakthrough curves of RO-16, RR-120 & RB-19 azo dyes in various concentrations. At lower concentrations, a gradient was developed, and the transport of azo dye pollutants from the aqueous medium decreased slowly (Alardhi *et al.*, 2020). Referring to that figures, a quick saturation point was observed at lower concentrations, and the breakthrough point was attained at very low concentrations. The saturation of the adsorbent bed was observed in 50 mg L^{-1} of azo dye concentrations, and after the breakthrough point, the azo dye uptake reached a constant rate. Azo dye adsorption increased when the concentration of azo dyes in the aqueous solutions was very low due to the driving forces in the mass transfer zone. Table 7 represents the values

obtained from breakthrough analysis by varying the concentration of azo dye solutions.

Table 5. Breakthrough analysis in various adsorbent bed heights

S.No	Azo dye type	Adsorbent bed height in cm	Break through time in min	Vol. of treated effluent in mL	Total flow time in min	Azo dyes were added in a column in min	Amount of azo dye adsorbed in mg	Bed capacity mg g^{-1}	% Removal
1.	RO - 16	5	550	13800	2750	1530	1124.7	237.52	78.42
2.		7.5	700	18500	3700	1850	1526.2	289.26	82.57
3.		10	1000	21500	4300	2150	1887.7	347.63	87.84
4.	RR - 120	5	600	17500	3500	1750	1034.2	203.36	59.18
5.		7.5	800	21000	4200	2100	1385.8	258.25	66.04
6.		10	1100	23500	4700	2350	1666.1	317.62	70.95
7.	RB - 19	5	400	15500	3100	1550	1236.6	213.72	79.78
8.		7.5	700	19500	3900	1950	1661.4	279.35	85.24
9.		10	1100	22500	4500	2250	2000.2	335.43	88.97

Table 6. Breakthrough analysis of various inflow rates of the solution

S.No	Azo dye type	Adsorbent bed height in cm	Break through time in min	Vol. of treated effluent in mL	Total flow time in min	Azo dyes were added in a column in min	Amount of azo dye adsorbed in mg	Bed capacity mg g^{-1}	% Removal
1.	RO - 16	5	1250	24300	4900	2420	2012.6	392.36	83.61
2.		7.5	1000	31500	4200	3150	2495.7	300.97	79.23
3.		10	700	37000	3700	3700	2875.6	225.3	77.72
4.	RR - 120	5	1100	24500	4900	2450	1745.3	348.88	71.24
5.		7.5	800	33000	4400	3300	2271.7	302.72	68.84
6.		10	500	39000	3900	3900	2618.8	224.83	67.15
7.	RB - 19	5	1100	23000	4600	2300	1884.3	376.46	80.19
8.		7.5	900	31500	4200	3150	2465.8	299.24	78.28
9.		10	700	38000	3800	3800	2932	214.89	77.16

Table 7. Breakthrough analysis in various azo dye concentrations

S.No	Azo dye type	Adsorbent bed height in cm	Break through time in min	Vol. of treated effluent in mL	Total flow time in min	Azo dyes were added in a column in min	Amount of azo dye adsorbed in mg	Bed capacity mg g^{-1}	% Removal
1.	RO - 16	100	1100	23500	4700	2350	1900.1	365.4	80.85
2.		200	900	21500	4300	4300	3280.9	436.8	76.32
3.		300	500	18500	3700	5550	3966.5	495.3	71.47
4.	RR -120	100	1200	23000	4600	2300	1670.2	340.8	72.62
5.		200	900	21500	4300	4300	2985.4	439.6	69.43
6.		300	600	16500	3300	4950	3309	378.1	66.85
7.	RB - 19	100	1300	24000	4800	2400	1950	410.5	81.25
8.		200	900	22000	4400	4400	3468.9	462.5	78.84
9.		300	600	19000	3800	5700	4415.7	496.1	76.53

3.9. Kinetic modelling

The mass transfer mechanism and performance of the fixed bed column have been assessed for real-world applications using various kinetic models. The following five kinds of kinetic models and their performance were evaluated in this process.

3.9.1. Thomas model

Similar to the breakthrough studies, the adsorption capacity and Thomas model constants 'q_o and K_{th}' were obtained by varying the bed height of the adsorbent, inflow rate of azo dye solution and concentration of dyes in the synthetic solutions. The experimental conditions in the column study were fitted with the model's regression values, indicating the model's applicability. The decrease in adsorption capacity may increase the Thomas model constants and inflow rate of the azo dye solutions (Dahr *et al.*, 2015). Also, the Thomas model constant 'K_{th}' were increased with the decrease in azo dye concentrations because of very high driving forces. When the adsorbent bed height is large, the adsorption capacity may increase, and a similar trend also developed at very high azo dye solution concentrations in the packed bed column (Selambakkannu *et al.*, 2019). The graphical representation

of Thomas model plots for azo dye solutions is shown in Figures 11 (a), (b), and (c), and the constants of this model were calculated from the slope and deflection values from the plot and are shown in Table 8.

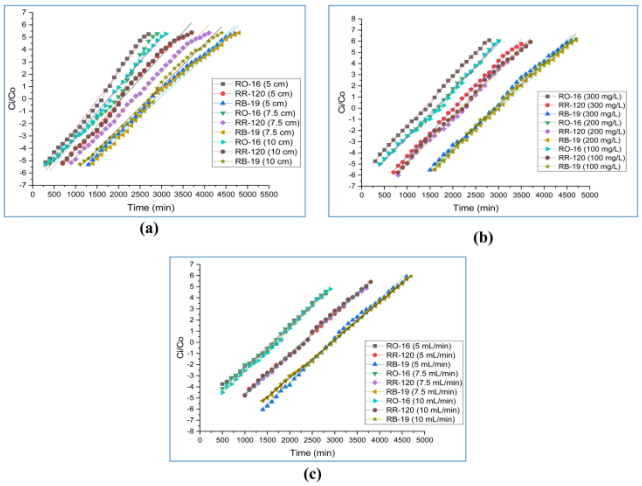

Figure 12. Yoon-Nelson model plots for (a) different bed depth, (b) azo dye concentration and (c) inflow rate of the synthetic solution in the packed bed column

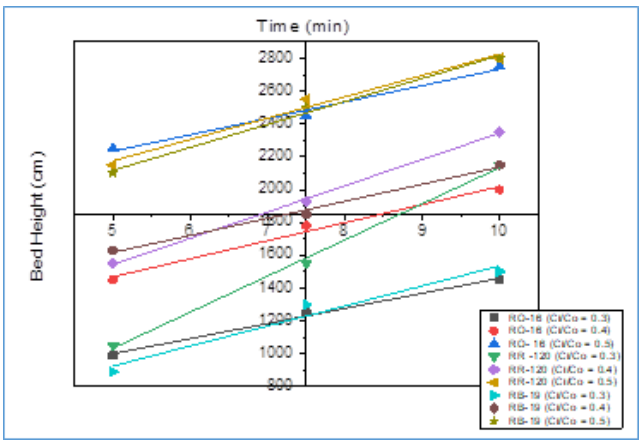

Figure 13. BDST model plots for RO-16, RR-120 & RB-19 azo dyes adsorption at various inlet and outlet concentrations of synthetic solutions in the packed bed column

3.9.2. Yoon – Nelson model

In this type of model, the time required to attain the breakthrough of 50% azo dyes adsorption (τ) and rate constant (K_{YN}) are the two important parameters that may be obtained by slope and deflection values from the linear plots of ln $[C_i / (C_o - C_i)]$ vs time (t). The flow rate of the azo dye solution, azo dye concentrations and adsorbent bed height were adjusted similar to the breakthrough studies. The values of the Yoon -Nelson model and its constants were obtained from the linear plots and represented in Table 9 & linear plots of this kinetic model shown in Figures 12 (a), (b), and (c) may confirm the applicability of this kinetic study. Referring to the straight line from the plots indicates the suitability of the Yoon-Nelson model, and the values of τ and K_{YN} are inversely proportional. This is because many azo dyes compete for the adsorbent surface at high amounts of dyes, which results in fast azo dyes absorption (Sirajudheen *et al.*, 2020).

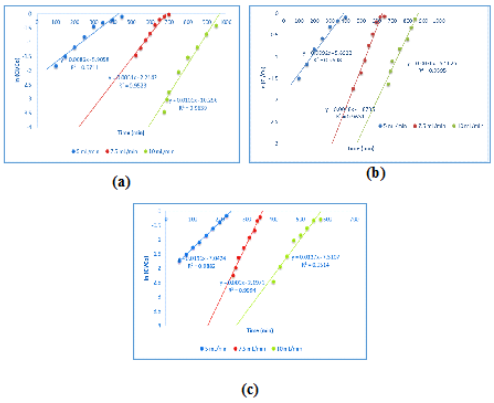

Figure 14. Adams-Bohart plots for the adsorption of RO-16, RR-120 & RB -19 azo dyes at the concentration of (a) 100 mg L^{-1}, (b) 200 mg L^{-1} & (c) 300 mg L^{-1} respectively

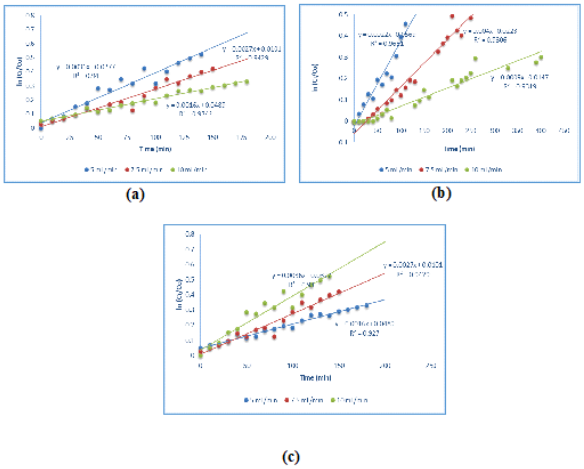

Figure 15. Wolborska plots for the adsorption of RO-16, RR-120 & RB -19 azo dyes at the concentration of (a) 100 mg L^{-1}, (b) 200 mg L^{-1} & (c) 300 mg L^{-1} respectively

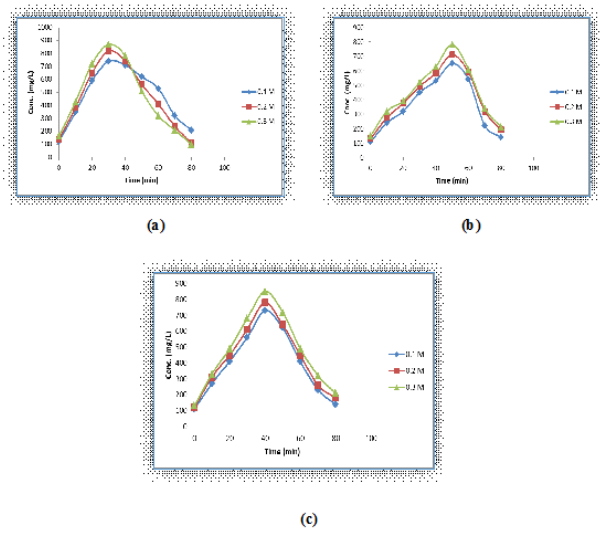

Figure 16. Desorption studies of azo dyes using concentrated sulfuric acid

3.9.3. BDST model

To reach the high amount of adsorption capacity, bed depth service time is an important parameter in the packed

bed column. The concentration of azo dyes was taken as a constant value. The BDST model helps to increase the azo dye uptake from the synthetic solutions (Saravanan *et al.*, 2017). Most azo dyes were adsorbed on the bed surface of sugarcane bagasse adsorbent, and the resistance of mass transfer and intra-particle diffusion are irrelevant. The service time of the adsorbent bed and its relationship with the height of the bed was represented by this model (Cervantes *et al.*, 2018). The model has been evaluated by varying the inlet and outlet concentrations by fixing the azo dye concentration of 50 mg L-1 and the inflow rate of azo dye solution into the column as 5 mL min-1. The linear plots of the BDST model are shown in Figure 13, and the constants of this model were obtained from the slope and deflection values from the plots and represented in Table 10. The linear plots show the applicability of the BDST model and its regression standards ($R^2 > 0.95$). Due to the very high accumulation of azo dyes on the adsorbent surface, there was an increase in the adsorption capacity per bed unit volume (N_o) with an increase in the inlet and outlet solution concentrations. Also, within 50% of inlet and outlet concentrations, the least regression value was obtained, which confirms the inlet and outlet concentrations may decrease the regression standards (Aydina *et al.*, 2021). There is a need for good inflow conditions and large adsorbent bed to attain the breakthrough earlier.

3.9.4. Adams-Bohart model

During the initial part of the breakthrough curve, the Adams-Bohrat model may be used to apply the experimental data for clear description. This model was used to estimate the maximum adsorption capacity (N_o) and kinetic constants (K_{AB}) and Figures 14 (a), (b), and (c) show the linear plots of the Adams-Bohrat model, which indicate the applicability of the kinetic model. Using the linear plots of ln (C_t/C_o) vs time, the values of N_o and K_{AB} were calculated by taking slope and intercept values and represented in Table 11. For this study, the flow rate was adjusted as 5 mL min^{-1}, 7.5 mL min^{-1} & 10 mL min^{-1} with a fixed adsorbent bed height of 10 cm and the concentration of azo dyes in the solution was adjusted from 100 – 300 mg L^{-1}. It was noticed that the increase in adsorbent bed height might decrease the constant of kinetics (K_{AB}) and increase the capacity of adsorption (N_o) for all three types of azo dyes. Because of higher active site availability at higher bed depths, adsorption capacity may be attributed to more. The prediction of the breakthrough curve was attained based on the regression values (R^2) obtained from the linear plots, and it was confirmed the suitability of the Adams-Bohrat model because of higher regression values ($R^2 > 0.95$).

Table 8. Thomas model constants for the adsorption of azo dyes using sugarcane bagasse powder

S. No.	Type of azo dye	Slope x10^{-3}	Intercept	Initial azo dye conc. x 10^2 mg L^{-1}	K_{th} x 10^{-5} min^{-1} mg^{-1} L^{-1}	Bed depth x 10^{-2} m	Flow rate L min^{-1}	q_o
1.		- 4.6	7.64	3	1.45	0.05	0.005	392.34
2.		-3.6	8.76	2	1.78	0.05	0.005	352.42
3.		-3.6	11.36	1	3.96	0.05	0.005	264.12
4.		-4.5	7.61	1	4.75	0.05	0.005	242.32
5.	RO - 16	-3.6	8.27	1	3.86	0.075	0.005	273.12
6.		-2.9	9.78	1	3.04	0.1	0.005	294.23
7.		-3.6	6.74	1	3.79	0.05	0.005	267.45
8.		-3.4	7.56	1	3.65	0.05	0.075	235.64
9.		-2.8	8.03	1	2.83	0.05	0.01	201.32
10.		-4.4	5.96	3	1.64	0.05	0.005	394.23
11.		-3.7	8.43	2	1.93	0.05	0.005	367.93
12.		-3.7	10.05	1	3.84	0.05	0.005	274.58
13.		-4.0	6.92	1	4.03	0.05	0.005	256.34
14.	RR-120	-3.7	8.03	1	3.69	0.075	0.005	275.92
15.		-3.5	9.14	1	3.48	0.1	0.005	298.58
16.		-3.5	6.12	1	3.45	0.05	0.005	273.29
17.		-3.6	8.14	1	3.69	0.05	0.075	248.56
18.		-3.0	8.73	1	3.16	0.05	0.01	212.13
19.		-4.2	7.69	3	1.54	0.05	0.005	392.83
20.		-4.1	8.72	2	2.73	0.05	0.005	338.48
21.		-3.7	9.14	1	3.54	0.05	0.005	274.93
22.		-3.9	7.68	1	3.93	0.05	0.005	241.36
23.	RB-19	-3.5	8.52	1	3.63	0.075	0.005	267.43
24.		-3.2	9.31	1	3.26	0.1	0.005	289.57
25.		-3.5	6.56	1	3.68	0.05	0.005	264.49
26.		-3.6	8.43	1	3.79	0.05	0.075	241.37
27.		-3.0	9.21	1	3.21	0.05	0.01	209.13

Table 9. Yoon-Nelson model constants for the adsorption of azo dyes using sugarcane bagasse powder

S. No.	Type of azo dye	Intercept	Initial azo dye conc. x 10^2 mg L^{-1}	K_{YN} x 10^{-3} min^{-1}	Bed depth x 10^{-2} m	Flow rate L min^{-1}	τ (min)
1.	RO-16	6.04	3	4.4	0.05	0.005	1532
2.		9.03	2	4.2	0.05	0.005	2112
3.		12.43	1	3.8	0.05	0.005	2894
4.		7.14	1	4.5	0.05	0.005	1724
5.		7.88	1	3.7	0.075	0.005	2047
6.		9.11	1	3.1	0.1	0.005	2756
7.		5.97	1	3.7	0.05	0.005	1765
8.		8.20	1	3.6	0.05	0.075	2384
9.		11.11	1	3.8	0.05	0.01	2965
10.	RR-120	6.87	3	4.2	0.05	0.005	1655
11.		9.05	2	4.1	0.05	0.005	2239
12.		11.41	1	3.8	0.05	0.005	3046
13.		7.49	1	4.2	0.05	0.005	1938
14.		8.18	1	3.5	0.075	0.005	2374
15.		9.42	1	3.2	0.1	0.005	2856
16.		6.03	1	3.8	0.05	0.005	1667
17.		8.41	1	3.7	0.05	0.075	2353
18.		10.05	1	3.4	0.05	0.01	2978
19.	RB-19	6.83	3	4.2	0.05	0.005	1763
20.		8.74	2	3.8	0.05	0.005	2256
21.		11.18	1	4.1	0.05	0.005	2948
22.		7.03	1	4.0	0.05	0.005	1864
23.		7.91	1	3.8	0.075	0.005	2436
24.		9.29	1	3.4	0.1	0.005	2743
25.		6.55	1	3.9	0.05	0.005	1759
26.		8.32	1	3.7	0.05	0.075	2362
27.		9.98	1	3.4	0.05	0.01	2984

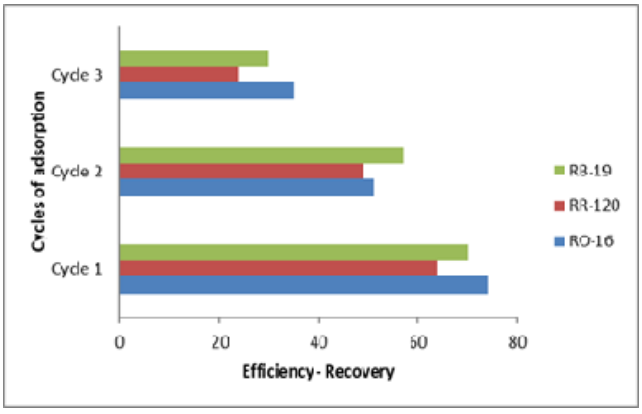

Figure 17. Regeneration of azo dyes using concentrated sulfuric acid in different cycles

3.9.5. Wolborska model

The experimental column data was applied to the Wolborska model to describe the breakthrough curves. The linear plots of ln (Ci/Co) vs time are shown in Figures 15 (a), (b), and (c), and the constants of this wolborska kinetic model (β_a & N_o) were determined by using slope and deflection values from the linear plots. Similar to the Adams – Bohart studies, the bed height was fixed, the azo dye concentration & inflow rate of the solution were adjusted, and the model's behaviour was evaluated. Based on the trial runs, kinetic model constants may be increased or decreased. The constants of this kinetic model are represented in Table 12, and there is no decrease from their original values. The active sites available on the sugarcane bagasse adsorbent were reduced on the surface for azo dye adsorption. The regression values (R^2) obtained from the linear plots are very low (<0.95), which shows the non-applicability of the wolborska model in this fixed bed adsorption study. Hence, the mass transfer mechanism in the adsorption process does not fit with this kinetic model (Benjelloun *et al.*, 2021). Out of five kinetic models tested for azo dyes adsorption, the Thomas, Yoon-Nelson, BDST & Adams-Bohart kinetic models fitted well with the experimental data in the fixed bed column.

3.10. Desorption studies

For azo dye solution, the elution curve of the fixed bed column is shown in Figure 16. The values of the maximum amount of desorption are represented in Table 13. During the initial stages, the desorption of azo dyes attained the maximum peak. After 30 minutes of desorption time, the rate of azo dye recovery decreased gradually for all three different types of sulfuric acid concentrations. The speed of removal rate from the adsorbent surface may be attributed to the sulfuric acid concentrations, which decrease the desorption rate (Himanshu Patel, 2021). The performance of the packed bed column has been evaluated based on the reuse of spent adsorbent material. Hence, the optimum

desorption time was fixed at 30 minutes, and the regeneration process was done in three different cycles. After reaching the saturation level of the adsorbent, the adsorbed pollutant was disposed into remote soil dumping process. Referring to Figure 17, the maximum amount of adsorbent was recovered in the first cycle; after that, the recovery rate was reduced significantly. Hence, the amount of spent adsorbent was recovered within 30 minutes by adding 0.3 N of concentrated sulfuric acid in the first cycle. No increase in azo dye recovery was observed when the sulfuric acid concentration went below 0.3 N.

Table 10. BDST model constants for the adsorption of azo dyes using sugarcane bagasse powder

S. No.	Type of azo dye	Bed depth x 10^{-2} m	Azo dye conc. in mg L^{-1}	C_i/C_o	Slope	Intercept	N_o mg L^{-1}	K x 10^{-5} L mg^{-1} min^{-1}	R^2
1.	RO - 16	0.05	100	0.3	110	540	49050	4.5	0.986
2.		0.075	100	0.4	100	918	53090	3.2	0.986
3.		0.10	100	0.5	92	1733	57340	2.1	0.994
4.	RR-120	0.05	100	0.3	220	66	45930	1.9	0.999
5.		0.075	100	0.4	160	743	51250	3.4	0.997
6.		0.10	100	0.5	130	1525	54640	2.4	0.982
7.	RB-19	0.05	100	0.3	140	315	47560	3.7	0.996
8.		0.075	100	0.4	122	1096	50540	3.3	0.962
9.		0.10	100	0.5	104	1416	53650	2.2	0.992

Table 11. Adams-Bohart constants for different azo dye concentrations

S. No.	Type of dye	Flow rate L min^{-1}	Initial azo dye conc. x 10^2 mg L^{-1}	Bed depth x 10^{-2} m	No mg L^{-1}	K_{AB} x 10^{-5} mL mg^{-1} min^{-1}	R^2
1.	RO - 16	0.05	3	1	2.25	5788.51	0.9711
2.		0.075	2	1	1.84	6438.24	0.9523
3.		0.10	1	1	1.52	8956.26	0.9639
4.	RR-120	0.05	3	1	2.73	5921.56	0.9698
5.		0.075	2	1	2.13	7345.24	0.9631
6.		0.10	1	1	1.75	9325.72	0.9595
7.	RB-19	0.05	3	1	2.56	5835.36	0.9882
8.		0.075	2	1	1.94	6593.52	0.9994
9.		0.10	1	1	1.62	9023.54	0.9514

Table 12. Wolborska model constants for different azo dye concentrations

S. No.	Type of dye	Flow rate L min^{-1}	Initial azo dye conc. x 10^2 mg L^{-1}	Bed depth x 10^{-2} m	β_a min^{-1}	R^2
1.	RO - 16	0.05	3	1	6.32	0.940
2.		0.075	2	1	7.84	0.9429
3.		0.10	1	1	9.28	0.9342
4.	RR-120	0.05	3	1	5.98	0.9651
5.		0.075	2	1	7.22	0.9306
6.		0.10	1	1	8.93	0.9319
7.	RB-19	0.05	3	1	6.12	0.940
8.		0.075	2	1	7.52	0.9429
9.		0.10	1	1	9.13	0.927

Table 13. Desorption rate of the adsorbent material in fixed bed column

S. No.	Type of azo dye	The concentration of H_2SO_4 (N)	Final Concentration mg L^{-1}	Time (min)
1.	RO-16	0.1	740	30
		0.2	820	
		0.3	870	
2.	RR-120	0.1	650	50
		0.2	710	
		0.3	780	
3.	RB-19	0.1	730	40
		0.2	780	
		0.3	850	

4. Conclusion

The sugarcane bagasse charcoal adsorbent was used to remove the RO-16, RB-120 and RB-19 azo dyes from the aqueous solutions. The characterization studies confirm the adsorption behaviour of prepared sugarcane bagasse adsorbent with the BET surface area of 654 m^2 g^{-1}. The maximum adsorption efficiency of 95% for RO-16, 88% for RR-120 and 82% for RB-19 dyes was achieved with the optimum pH of 6.0, Sugarcane bagasse dose of 2.5 g L^{-1}, azo dye concentration of 25 mg L^{-1} and the temperature of 30°C. The analysis data were fitted with the Langmuir and Freundlich isotherm models. The packed bed column study confirms the earlier breakthrough at 10 cm of adsorbent bed height, 5 mL min^{-1} inflow rate into the column and 100 mg L^{-1} of azo dye concentrations. The column analysis data are fitted well with Thomas, Yoon-Nelson, BDST and Adams-Bohart kinetic studies, and 0.3 N of sulfuric acid provides a very high desorption rate from the column at the earlier time. Based on the experimental process, the sugarcane bagasse charcoal adsorbent confirmed its adsorption behaviour of azo dyes from the aqueous solutions.

References

Adeyemo A.A., Adeoye I.O., and Bello O.S. (2015). Adsorption of dyes using different types of clay: a review, *Applied Water Science*, **7**, 543–568. https://doi.org/10.1007/s13201-015-0322-y.

Alardhi S.M., Albayati T.M., and Alrubay J.M. (2020). Adsorption of the methyl green dye pollutant from aqueous solution using mesoporous materials MCM-41 in a fixed-bed column, *Heliyon*, **6**(1), e03253. https://doi.org/10.1016/j.heliyon.2020.e03253.

Al-Senani G.M. and Al-Fawzan F.F. (2018). Adsorption study of heavy metal ions from aqueous solution by nanoparticle of wild herbs, *The Egyptian Journal of Aquatic Research*, **44**(3), 187–194. https://doi.org/10.1016/j.ejar.2018.07.006.

Ambaye T.G., Vaccari M., van Hullebusch E.D., Amrane A., and Rtimi S. (2021). Mechanisms and adsorption capacities of biochar for the removal of organic and inorganic pollutants from industrial wastewater, *International Journal of Environmental Science and Technology*, **18**, 3273–3294. https://doi.org/10.1007/s13762-020-03060-w.

Amiri M.J., Khozaei M., and Gil A. (2019). Modification of the Thomas model for predicting unsymmetrical breakthrough curves using an adaptive neural-based fuzzy inference system, *Journal of Water & Health*, **17**(1), 25–36. https://doi.org/10.2166/wh.2019.210.

Aydına S., Nura H.M., Traorea A.M., Yıldırımb E., and Emik S. (2021). Fixed bed column adsorption of vanadium from water using amino-functional polymeric adsorbent, *Desalination and Water Treatment*, **209**, 280–288. 10.5004/dwt.2021.26493.

Banerjee S., and Chattopadhyaya M.C. (2017). Adsorption characteristics for the removal of a toxic dye, tartrazine from aqueous solutions by a low-cost agricultural by-product, *Arabian Journal of Chemistry*, **10**, S1629–S1638. https://doi.org/10.1016/j.arabjc.2013.06.005.

Bazan A., Nowicki P., Półrolniczak P., and Pietrzak R. (2016). Thermal analysis of activated carbon obtained from residue after supercritical extraction of hops, *Journal of Thermal Analysis and Calorimetry*, **125**, 1199–1204. https://doi.org/10.1007/s10973-016-5419-5.

Benabela I., Benderrag A., Haddou B., Canselier J.P. and Gourdon C. (2022). Dye removal with emulsion liquid membrane: experimental design and response surface methodology, *Environmental Technology*. https://doi.org/10.1080/09593330.2022.2091480.

Benjelloun M., Miyah Y., Evrendilek G.A., Lairini F.Z.S. (2021). Recent advances in adsorption kinetic models: their application to dye types, Arabian *Journal of Chemistry*, **14**(4), 103031. https://doi.org/10.1016/j.arabjc.2021.103031.

Biz l., Finkler A.T.J., Pitol L.O., Medina B.S., Krieger N., and Mitchell D.A. (2016). Production of pectinases by solid-state fermentation of a mixture of citrus waste and sugarcane bagasse in a pilot-scale packed-bed bioreactor, *Biochemical Engineering Journal*, **111**, 54–62. https://doi.org/10.1016/j.bej.2016.03.007.

Briffa J., Sinagra E., and Blundell R. (2020). Heavy metal pollution in the environment and their toxicological effects on humans, *Heliyon*, **6**(9), e04691. https://doi.org/10.1016/j.heliyon.2020.e04691.

Dey A.K., Dey A., and Goswami R. (2022). Adsorption characteristics of methyl red dye by Na2CO3-treated jute fibre using multi-criteria decision-making approach, *Applied Water Science*, **12**, 179. https://doi.org/10.1007/s13201-022-01700-9.

Dittmann D., Saal L., Zietzschmann F., Mai M., Altmann K., Al-Sabbagh D., Schumann P., Ruhl A.S., Jekel M. and Braun U. (2022). Characterization of activated carbons for water treatment using TGA-FTIR for analysis of oxygen-containing functional groups, *Applied Water Science*, **12**, 203. https://doi.org/10.1007/s13201-022-01723-2.

Djelloul C., and Hamdaoui O. (2014). Dynamic adsorption of methylene blue by melon peel in fixed-bed columns, *Desalination and Water Treatment*, **56**, 2966–2975. https://doi.org/10.1080/19443994.2014.963158 .

El-Naas M.H., Alhaija M. A., and Al-Zuhair S. (2017). Evaluation of an activated carbon packed bed for the adsorption of phenols from petroleum refinery wastewater, *Environmental Science and Pollution Research*, **24**, 7511–7520. https://doi.org/10.1007/s11356-017-8469-8.

Fideles R.A., Teodoro F.S., Xavier A.L.P., Adarme O.F.H., Gil L.F., and Gurgel L.V.A. (2019). Trimellitated sugarcane bagasse: A versatile adsorbent for removal of cationic dyes from aqueous solution. Part II: Batch and continuous adsorption in a bicomponent system, *Journal of Colloid and Interface Science*, **552**(15), 752–763. https://doi.org/10.1016/j.jcis.2019.05.089.

Foroughi-dahr M., Esmaieli M., Abolghasemi H., Shojamoradi A. and Pouya E.S. (2015). Continuous adsorption study of congo red using tea waste in a fixed-bed column, *Desalination and Water Treatment*, **57**(18), 8437–8446. https://doi.org/10.1080/19443994.2015.1021849.

Gisi S.D., Lofrano G., Grassi M. and Notarnicola M. (2016). Characteristics and adsorption capacities of low-cost sorbents for wastewater treatment: A review, *Sustainable Materials*

and Technologies, **9**, 10–40. https://doi.org/10.1016/j.susmat.2016.06.002.

Gisi S.D., Lofrano G., Grassi M., and Notarnicola M. (2016). Characteristics and adsorption capacities of low-cost sorbents for wastewater treatment: A review, *Sustainable Materials and Technologies*, **9**, 10–40. https://doi.org/10.1016/j.susmat.2016.06.002.

Guo Y., Tan C., Sun J., Li W., Zhang J. and Zhaoa C. (2020). Porous activated carbons derived from waste sugarcane bagasse for CO2 adsorption, *Chemical Engineering Journal*, 381, 122736. https://doi.org/10.1016/j.cej.2019.122736.

Harripersadth C., Musonge P., Isa Y.M., Morales M.G. and Sayago A. (2020). The application of eggshells and sugarcane bagasse as potential biomaterials in the removal of heavy metals from aqueous solutions, *South African Journal of Chemical Engineering*, **34**, 142–150. https://doi.org/10.1016/j.sajce.2020.08.002.

Juela D., Vera M., Cruzat C., Alvarez X. and Vanegas E. (2021). Adsorption properties of sugarcane bagasse and corn cob for the sulfamethoxazole removal in a fixed-bed column, *Sustainable Environment Research*, **31**, 27. https://doi.org/10.1186/s42834-021-00102-x.

Kaya N. (2017). A comprehensive study on adsorption behavior of some azo dyes from aqueous solution onto different adsorbents, *Water Science & Technology*, **76**(2), 478–489. https://doi.org/10.2166/wst.2017.216.

Kepenek E.S., Severcan M., Gozen A.G. and Severcan F. (2020). Discrimination of heavy metal acclimated environmental strains by chemometric analysis of FTIR spectra, *Ecotoxicology and Environmental Safety*, **202**, 110953. https://doi.org/10.1016/j.ecoenv.2020.110953.

Kerrou M., Bouslamti N., Raada A., Elanssari A., Mrani D. and Slimani M.S. (2021). The use of sugarcane bagasse to remove the organic dyes from wastewater, *International Journal of Analytical Chemistry*, ID: 5570806. https://doi.org/10.1155/2021/5570806.

Khamparia S., and Jaspal D. (2016). Adsorptive removal of Direct Red 81 dye from aqueous solution onto Argemone Mexicana, *Sustainable Environment Research*, **26**(3), 117–123. https://doi.org/10.1016/j.serj.2016.04.002.

Khoo E-C., Ong S-T., and Ha S-T. (2012). Removal of basic dyes from aqueous environment in single and binary systems by sugarcane bagasse in a fixed-bed column, *Desalination and Water Treatment*, **37**, 215–222. https://doi.org/10.1080/19443994.2012.661275.

Krishna Murthy T.P., and Gowrishankar B.S. (2020). Process optimization of methylene blue sequestration onto physical and chemical treated coffee husk-based adsorbent, *SN Applied Sciences*, **2**, 836. https://doi.org/10.1007/s42452-020-2603-9.

Li Y., Zhang Q., Zhang J., Jin L., Zhao X., and Xu T. (2015). A top-down approach for fabricating free-standing bio-carbon supercapacitor electrodes with a hierarchical structure, *Scientific Reports*, **5**, 14155. https://doi.org/10.1038/srep14155.

Liu P., Zhang H., Xiang H., and Yan Y. (2016). Adsorption separation for high purity propane from liquefied petroleum gas in a fixed bed by removal of alkanes, *Separation and Purification Technology*, **158**, 1–8. https://doi.org/10.1016/j.seppur.2015.12.003.

López-Cervantes J., Sánchez-Machado D.I., Sánchez-Duarte R.G., and Correa-Murrieta M.A. (2018). Study of a fixed-bed column in the adsorption of an azo dye from an aqueous medium using a chitosan– glutaraldehyde biosorbent, *Adsorption Science & Technology*, **36**(1–2), 215–232. Doi: 10.1177/0263617416688021.

Nippes R.P., Macruz P.D., Molina L.C.A. and Scaliante M.H.N.O. (2022). Hydroxychloroquine adsorption in aqueous medium using clinoptilolite Zeolite, *Water, Air, & Soil Pollution*, **233**, 287. https://doi.org/10.1007/s11270-022-05787-3.

Patel H. (2021). Review on solvent desorption study from exhausted adsorbent, *Journal of Saudi Chemical Society*, **25**(8), 101302. https://doi.org/10.1016/j.jscs.2021.101302.

Ramasamy L., and Miranda L.R. (2022). Surface-modified adsorbent from artocarpus heterophyllus lam biomass to confine reactive Red 194 in real and synthetic effluents: kinetics and equilibrium study, Adsorption *Science and Technology*, ID: 4129833. https://doi.org/10.1155/2022/4129833.

Saad D.M., Cukrowska E. and Tutu H. (2015). Column adsorption studies for the removal of U by phosphonated cross-linked polyethylenimine: modelling and optimization, *Applied Water Science*, **5**, 57–63. https://doi.org/10.1007/s13201-014-0162-1.

Saadi R., Saadi Z., Fazaeli R. and Fard N.E. (2015). Monolayer and multilayer adsorption isotherm models for sorption from aqueous media, *Korean Journal of Chemical Engineering*, **32**, 787–799. https://doi.org/10.1007/s11814-015-0053-7.

Saleem J., Shahid U.B., Hijab M., Mackey H., and McKay G. (2019). Production and applications of activated carbons as adsorbents from olive stones, *Biomass Conversion and Biorefinery*, **9**, 775–802. https://doi.org/10.1007/s13399-019-00473-7.

Saravanan A., Senthil Kumar P., and Yaswanthraj M. (2017). Modeling and analysis of a packed-bed column for the effective removal of zinc from aqueous solution using dual surface-modified biomass, *Particulate Science and Technology*, **36**(8), 934–044. https://doi.org/10.1080/02726351.2017.1329243.

Saruchia and Kumar V. (2019). Adsorption kinetics and isotherms for the removal of rhodamine B dye and Pb+2 ions from aqueous solutions by a hybrid ion-exchanger, *Arabian Journal of Chemistry*, **12**(3), 316–329. https://doi.org/10.1016/j.arabjc.2016.11.009.

Sathya K., Nagarajan K., Carlin Geor Malar G., Rajalakshmi S., and Raja Lakshmi P. (2022). A comprehensive review on comparison among effluent treatment methods and modern methods of treatment of industrial wastewater effluent from different sources, *Applied Water Science*, **12**, 70. https://doi.org/10.1007/s13201-022-01594-7.

Selambakkannu S., Othman N.A.F., Bakar K.A., and Karim Z.A. (2019). Adsorption studies of packed bed column for the removal of dyes using amine functionalized radiation induced grafted fiber, *SN Applied Sciences*, **1**, 175. https://doi.org/10.1007/s42452-019-0184-2.

Sharifian S. and Asasian-Kolur N. (2020). Semiempirical investigation of Hg adsorption process in a continuous mode, *Indian Chemical Engineer*, **64**(1), 42–56. https://doi.org/10.1080/00194506.2020.1773939.

Shindhal T., Rakholiya P., Varjani S., Pandey A., Ngo H.H., Guo W., Ng H.Y., and Taherzadeh M.J. (2020). A critical review on advances in the practices and perspectives for the treatment

of dye industry wastewater, *Bioengineered*, **12**(1), 70–87. https://doi.org/10.1080/21655979.2020.1863034.

Sirajudheen P., Karthikeyan P., Basheer M.C., and Meenakshi S. (2020). Adsorptive removal of anionic azo dyes from effluent water using Zr (IV) encapsulated carboxymethyl cellulose-montmorillonite composite, *Environmental Chemistry and Ecotoxicology*, **2**, 73–82. https://doi.org/10.1016/j.enceco.2020.04.002.

Staszewski T., Borowko M. and Boguta P. (2022). Adsorption of Polymer-Tethered Particles on Solid Surfaces, *The Journal of Physical Chemistry-B*, **126**(6), 1341–1351. https://doi.org/10.1021/acs.jpcb.1c10418.

Sultana M., Rownok M.H., Sabrin M., Md Hafezur Rahaman and Nur Alama S.M. (2022). A review on experimental chemically modified activated carbon to enhance dye and heavy metals adsorption, *Cleaner Engineering and Technology*, **6**, 100382. https://doi.org/10.1016/j.clet.2021.100382.

Tahir H., Sultan M., Akhtar N., Hameed U., and Abid T. (2016). Application of natural and modified sugar cane bagasse for the removal of dye from aqueous solution, *Journal of Saudi Chemical Society*, **20**(1), S115–S121. https://doi.org/10.1016/j.jscs.2012.09.007.

Tzabar N. and ter Brake H.J.M. (2016). Adsorption isotherms and Sips models of nitrogen, methane, ethane, and propane on commercial activated carbons and polyvinylidene chloride, *Adsorption*, **22**, 901–914. https://doi.org/10.1007/s10450-016-9794-9.

Venkatraman Y., and Priya A.K. (2021). Removal of heavy metal ion concentrations from the wastewater using tobacco leaves coated with iron oxide nanoparticles, *International Journal of Environmental Science and Technology*, **19**, 2721–2736. https://doi.org/10.1007/s13762-021-03202-8.

Xiao H., Zhaoa T., Li C-H., and Lia M-Y. (2017). Eco-friendly approaches for dyeing multiple type of fabrics with cationic reactive dyes, *Journal of Cleaner Production*, 165, 1499–1507. https://doi.org/10.1016/j.jclepro.2017.07.174.

Yaseen D. A. and Scholz M. (2018). Textile dye wastewater characteristics and constituents of synthetic effluents: a critical review, *International Journal of Environmental Science and Technology*, **16**, 1193–1226. https://doi.org/10.1007/s13762-018-2130-z.

Yu J-X., Zhu J., Feng L-Y., Cai X-L., Zhang Y-F. and Chi R. (2019). Removal of cationic dyes by modified waste biosorbent under continuous model: Competitive adsorption and kinetics, *Arabian Journal of Chemistry*, **12**(8), 2044–2051. https://doi.org/10.1016/j.arabjc.2014.12.022.

Zafar M.N., Dar Q., Nawaz F., Zafar M.N., Iqbal M. and Nazar M.F. (2019). Effective adsorptive removal of azo dyes over spherical ZnO nanoparticles, *Journal of Materials Research and Technology*, **8**(1), 713–725. https://doi.org/10.1016/j.jmrt.2018.06.002.